minerals

MDPI

Article

Origin of the Dolomitic Ooids Formed in the Pliocene Shizigou Formation in the Qaidam Basin, Northern Tibet Plateau and Implications for Climate Change

Lewei Hao [1,2], Jiantuan Jia [3,4,*], Huifei Tao [1,2,*], Jinniu Chen [3,4], Xiaofeng Ma [1,2], Shutong Li [1] and Junli Qiu [1]

[1] Key Laboratory of Petroleum Resources, Northwest Institute of Eco-Environment and Resources, Chinese Academy of Sciences, Lanzhou 730000, China
[2] National Engineering Research Center of Offshore Oil and Gas Exploration, Beijing 100028, China
[3] Qaidam Comprehensive Geological and Mineral Exploration Institute of Qinghai Province, Golmud 816099, China
[4] Key Laboratory of Salt Lake Resource Exploration and Research in Qaidam Basin of Qinghai Province, Golmud 816099, China
* Correspondence: czy@qhczy.cn (J.J.); taohuifei@nieer.ac.cn (H.T.)

Abstract: The concentric layers of ooids from the modern environment are mostly aragonite and those from the ancient are mostly calcite and Mg-calcite. Dolomitic ooids are rare and are usually formed via the replacement of aragonite or calcite. Here, dolomitic ooids were found in the Pliocene Shizigou Formation in the Qaidam Basin, Northern Tibet Plateau. This paper focuses on whether the dolomitic ooids is a primary precipitate. Optical microscope and scanning electron microscope observation, combined with X-ray diffraction and cathodoluminescence analyses, indicate that the primary mineral of the ooid cortices is poorly ordered dolomite. Extracellular polymeric substances and pyrite were found in the ooids, indicating that the microbe participation was involved in the formation of the ooids. Firstly, the ooids grow on the offshore lake floor. Due to the involvement of sulfate-reducing bacteria and dissolved silica, the nanominerals were precipitated on extracellular polymeric substances. Then, the ooids were transported to strong hydrodynamic surf zones, where the random nanominerals were abraded to form flattened plates as a new polished layer. In addition, a comparison between the carbon and oxygen isotopic compositions and minerals of ooids from different periods indicate that the Pliocene lakes had a lower salinity and were more humid than Pleistocene lakes. Therefore, ooids may be an effective proxy for reflecting the climatic change and uplift history of the Tibet Plateau.

Keywords: ooids; salt lake; sulfate-reducing bacteria; Pleistocene; Qaidam Basin

Citation: Hao, L.; Jia, J.; Tao, H.; Chen, J.; Ma, X.; Li, S.; Qiu, J. Origin of the Dolomitic Ooids Formed in the Pliocene Shizigou Formation in the Qaidam Basin, Northern Tibet Plateau and Implications for Climate Change. *Minerals* **2022**, *12*, 1586. https://doi.org/10.3390/min12121586

Academic Editor: Aleksey Sadekov

Received: 14 November 2022
Accepted: 9 December 2022
Published: 10 December 2022

1. Introduction

Ooids are spherical or ellipsoidal grains with concentric layers of carbonate, which accrete around a nucleus composed of a material such as a lithoclast, bioclast, or siliciclastic grain [1]. Ooids are found in both ancient and modern sedimentary environments [2–5]. However, whether the formation of ooids is an inorganic or organic process has been debated over several centuries. The widely accepted theory is that the formation is attributed to a physicochemical process, which emphasizes the formation of inorganic carbonates through direct chemical precipitation from water [6,7]. Recently, by applying new technologies and integrative approaches, it has been suggested that microbes play a key role in the formation of ooids [8–12]. Metabolic activities can change the water chemical condition, leading to carbonate mineral formation [8,9]. Although the origin of ooids is controversial, they contain abundant geochemical and petrographic information. Thus, ooids can be used as paleoclimatic and paleoceanographic proxies that reflect the water

temperature, chemistry, redox state, salinity, and carbonate saturation state of their environment [13–16]. The mineral compositions of ooids may undergo variations through geological history [17]. Aragonitic layers dominate in modern ooids, whereas the concentric layers of ancient ooids are mostly composed of calcite and Mg-calcite [17,18]. The primary mineral of ooids may further provide a more accurate clue to understand paleo-water chemistry [17]. In order to reconstruct the paleoenvironmental conditions, the identification of an ooid's primary mineral is necessary.

Here, we report the first discovery of dolomitic ooids in the Pliocene Shizigou Formation from the Qaidam Basin. Combining X-ray diffraction data, scanning electron microscope (SEM) observations, and carbon and oxygen isotopic compositions of the ooids, the primary mineral of the ooids was identified to be dolomite, and its origin is discussed. The Qaidam Basin lies in the northeastern Tibetan Plateau, which deposits thick layer of Cenozoic lake sediments and has recorded tectonic and climatic changes since the Paleocene epoch [19]. Previous studies have focused on geochemical, magnetic, mineral, grain size, and paleontology to study the climatic changes of the Qaidam Basin [19–23]. The climatic change and uplift history of the Qaidam Basin could have led to the oscillations of minerals by controlling the depositional environment [20]. Aragonitic ooids were often formed in the Pleistocene [23,24], but ooids are less reported in the Pliocene. In this study, we discovered dolomitic ooids in the Pliocene Shizigou Formation, which are different from the ooids formed in the Pleistocene. By discussing the origin of dolomitic ooids and comparing them with the ooids developed in the Pleistocene, it can be determined whether the ooids can reflect the climatic change and uplift history of the Tibet Plateau.

2. Study Area

The Qaidam Basin, located on the northeastern Tibetan Plateau (Figure 1a), is a large intermountain basin (~700 km × 300 km) [25]. It is surrounded by the Kunlun Mountains to the south, the Qilian Mountains to the north, and the Altyn Mountains to the northwest (Figure 1b). The basin sits at an elevation of 2800–3300 m and is a vast arid region [25]. The basin's annual evaporation is over 20 times greater than its annual precipitation [21]. The mean annual temperature is about 0–5 °C [23]. The Qaidam Basin is the largest Cenozoic sedimentary basin within the Tibetan plateau [26]. Its formation was closely related to the India–Asia collision. The Cenozoic tectonic evolution history of the Qaidam Basin underwent three stages: the strike-slip basin stage (60–46 Ma), the foreland basin development (46–2.4 Ma), and the intermontane basin stage (2.45–0 Ma) [27]. The Cenozoic strata in the Qaidam Basin exceed a thickness of 12,000 m [19], and were deposited mainly in a fluvial-lacustrine environment that includes alluvial fans and fluvial, delta and lake sediments [28]. This Cenozoic stratigraphy can be divided into the following seven formations: the Lulehe Formation (E_{1+2}), the Xiaganchaigou Formation (E_3), the Shanganchaigou Formation (N_1), the Xiayoushashan Formation (N_2^1), the Shangyoushashan Formation (N_2^2), the Shizigou Formation (N_2^3), and the Qigequan Formation (Q_1) [19,29]. This study area lies on the Yahu Anticline, located in the central Qaidam Basin (Figure 1b). At this study location, the Shizigou Formation (5.2 Ma to 2.6 Ma) is dominated by marginal lakes and mud-flat environments with fluvial contribution [30]. The Qigequan Formation is dominated by evaporite lithofacies [30]. A well, Z1, was drilled in this area and a sample (Z1-15) was collected from the Shizigou Formation at a depth of 1500 m (Figure 2).

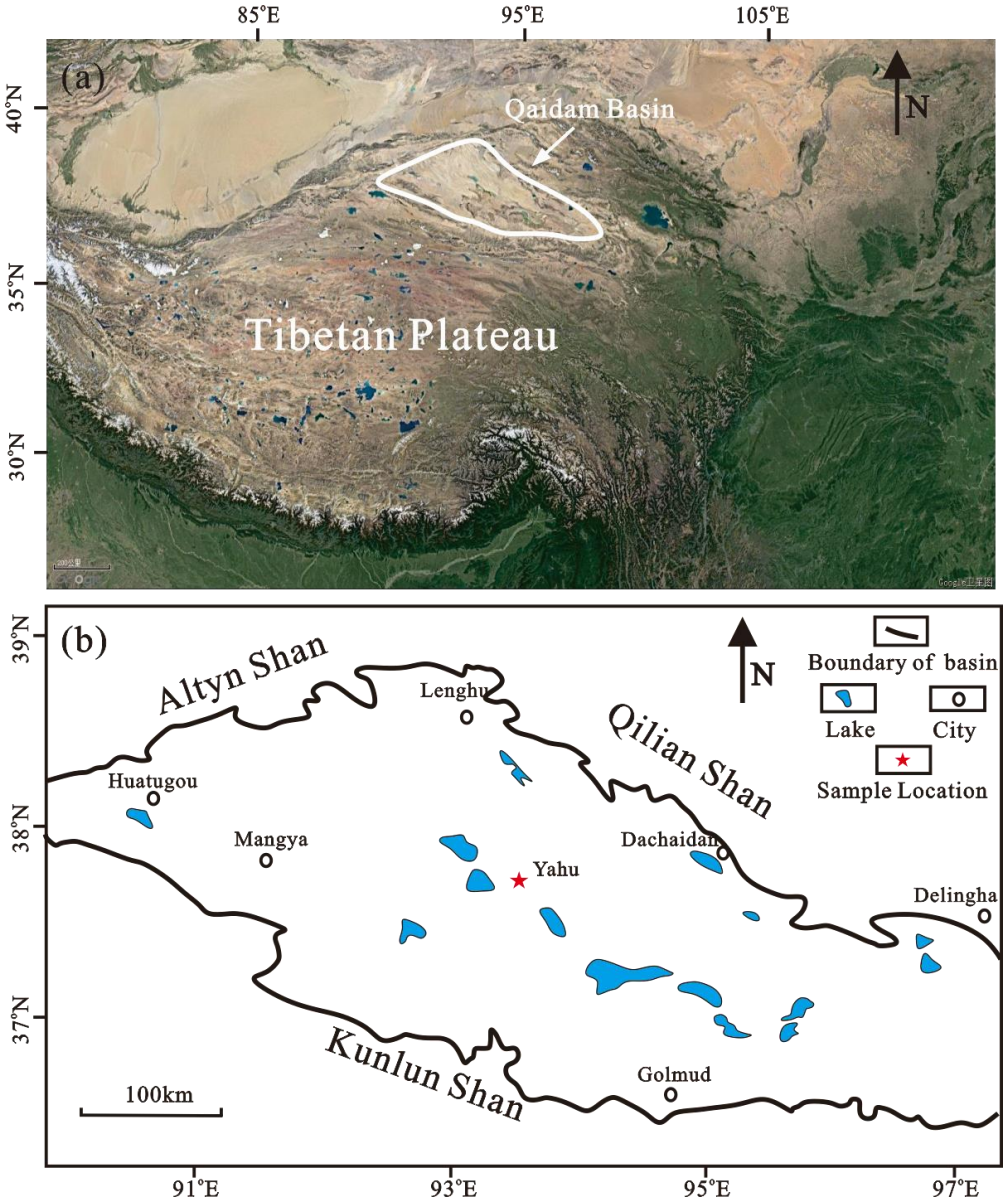

Figure 1. Location of the study area. (**a**) location of the Qaidam Basin; (**b**) location of the sample in the Qaidam Basin. Satellite image taken from Google Earth.

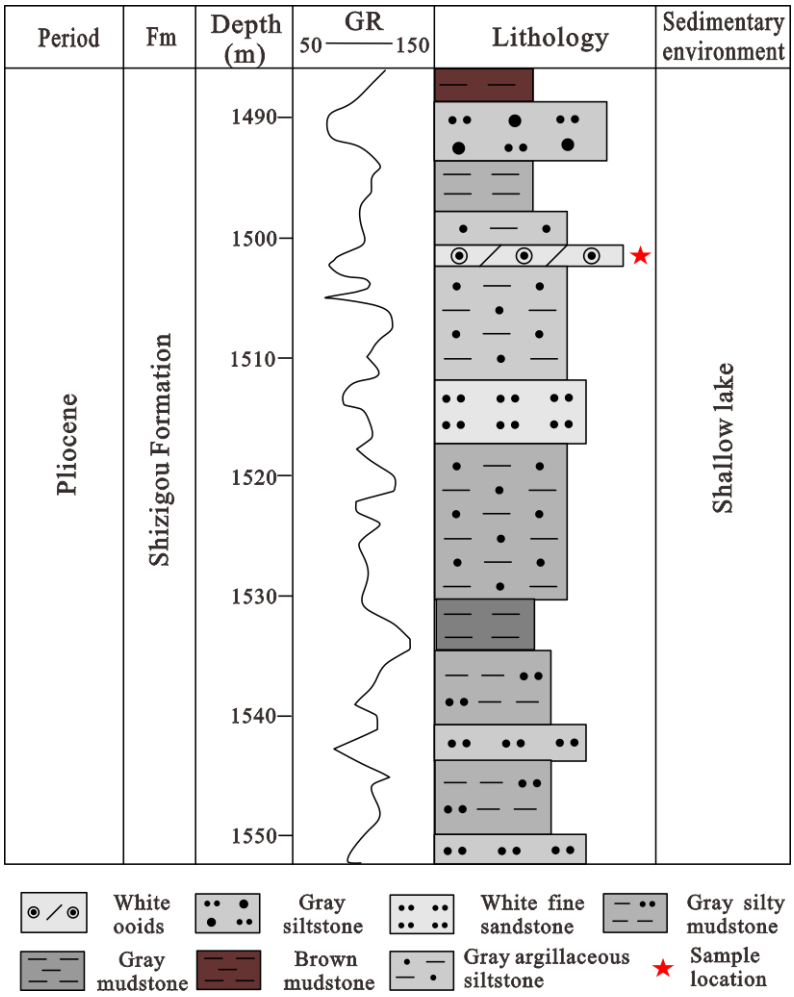

Figure 2. Sedimentological and petrophysical characteristics of the well Z1.

3. Materials and Methods

The sample Z1-15 was divided into three parts (A1, A2 and A3) for different analyses. Sample A1 was used for optical microscope and cathodoluminescence observations. Two polished thin sections were prepared from sample A1. One section was stained with Alizarin Red S and K ferricyanide and was imaged under a polarization microscope with a photo-collecting system (Zeiss Axioscope A1 APOL). The other section was used for cathodoluminescence (CL) analyses using an Olympus microscope equipped with a CL8200-MKSCLinstrument. To acquire more microinformation about the sample, sample A2 was used for SEM observation. Two polished thin sections and one fresh section were prepared for SEM. One thin section was prepared via Ar ion milling (685.C, Hitachi High-Tech) with an accelerating voltage of 5 kV and a milling time of 0.5 h. The other thin section and the fresh section were coated with carbon to render them conductive. Three sections were mounted on aluminium stubs and imaged using a Zeiss MERLIN Compact field emission scanning electron microscope (FESEM) with an X-ray energy dispersive spectrometer (EDS) (Xflash/30, Bruker). Lower accelerating voltages (1 kV) with working distances of approximately 5mm were used on the thin section milled by Ar ion. The other thin section and the fresh section were observed using the higher accelerating voltages of 5 kv, 10 kv, or 15 kv, and working distances of about 8 mm. Both secondary electron (SE) and angle-selective backscatter (ASB) images were acquired. The ooid size and cortical thickness were obtained from SEM micrograph images using the ImageJ software.

Sample A3 was crushed into 200 mesh powders by using an agate mortar for carbon and oxygen stable isotope analyses and whole-rock minerals. A minor amount of powders reacted with 100% orthophosphate at a temperature of 90°C to obtain CO_2. The carbon

and oxygen isotope compositions of CO_2 were analyzed using a Thermo Fisher Delta V-GasBench II mass spectrometer. Carbon and oxygen isotope compositions of samples were expressed with respect to the Vienna PeeDee Belemnite (V-PDB) standards. Replicate measurements of the standard were 0.06‰ for $\delta^{13}C$ and 0.08‰ for $\delta^{18}O$. Whole-rock minerals were analyzed using a Rigaku Ultima IV X-ray diffraction (XRD) analyzer with Cu-Kα radiation, a voltage of 40kV, and a current of 40 mA. The quartz (d_{101} = 3.343 Å) was used as an inter-standard to correct the peak. The ratio of the intensity of the (015) reflection to the (110) reflection (R) was used for estimating the degree of cation ordering in the dolomite [31]. The Mg content of the dolomite was calculated by using the method of a diagram of $MgCO_3$ % vs. d_{104}, which was constructed by Fang and Xu [32].

4. Results

4.1. Mineralogy

The XRD patterns show that the sample is constituted of dolomite and calcite (Figures 3 and S1). The (104) plane *d*-spacing (d_{104}) in the calcite of the sample is 3.029 Å. According to the method for calculating the Mg content of the calcite [32,33], the value of $MgCO_3$ is only 1.9 mol%. Generally, calcites containing >4 mol% $MgCO_3$ are considered to be high-magnesium calcite, and, conversely, those containing <4 mol% $MgCO_3$ are called low-magnesium calcite [34]. A linear relationship exists between the increase Mg^{2+} content and the decrease in the (104) *d*-spacing (larger 2θ value) in calcites [35]. Figure 3 shows that the (104) reflection in the sample (Figure 3c) is located between optical-grade calcite (Figure 3d) and high-magnesium calcite (Figure 3b). Thus, the calcite in the sample is considered to be low-magnesium calcite.

The (015) reflection is the most intense "ordering" reflection (indicating alternating layers of Mg and Ca) observed out of all the dolomite XRD patterns (Figure 3a) [36]. The (015) reflection displays decreasing intensity alongside disorder [31]. The ordered, stoichiometric dolomite shows nearly equal intensities between the two reflections (R = 1) in the XRD patterns (Figure 3a). The (015) reflection in this sample has a weak intensity (Figure 3c). The ordering state of the dolomite in this sample is 0.11, which means it is poorly ordered. The d_{104} of the dolomite of the sample is 2.912 Å. The Mg content of the dolomite was calculated by using the diagram of $MgCO_3$ % vs. d_{104} [32]. When the d_{104} is 2.912 Å, the content of Mg ranges from 40 mol% to 55 mol% and is constrained by the lowest and highest cation ordering state. Combined with the order parameter of 0.11, the Mg content of the dolomite in the sample is about 50.5 mol%.

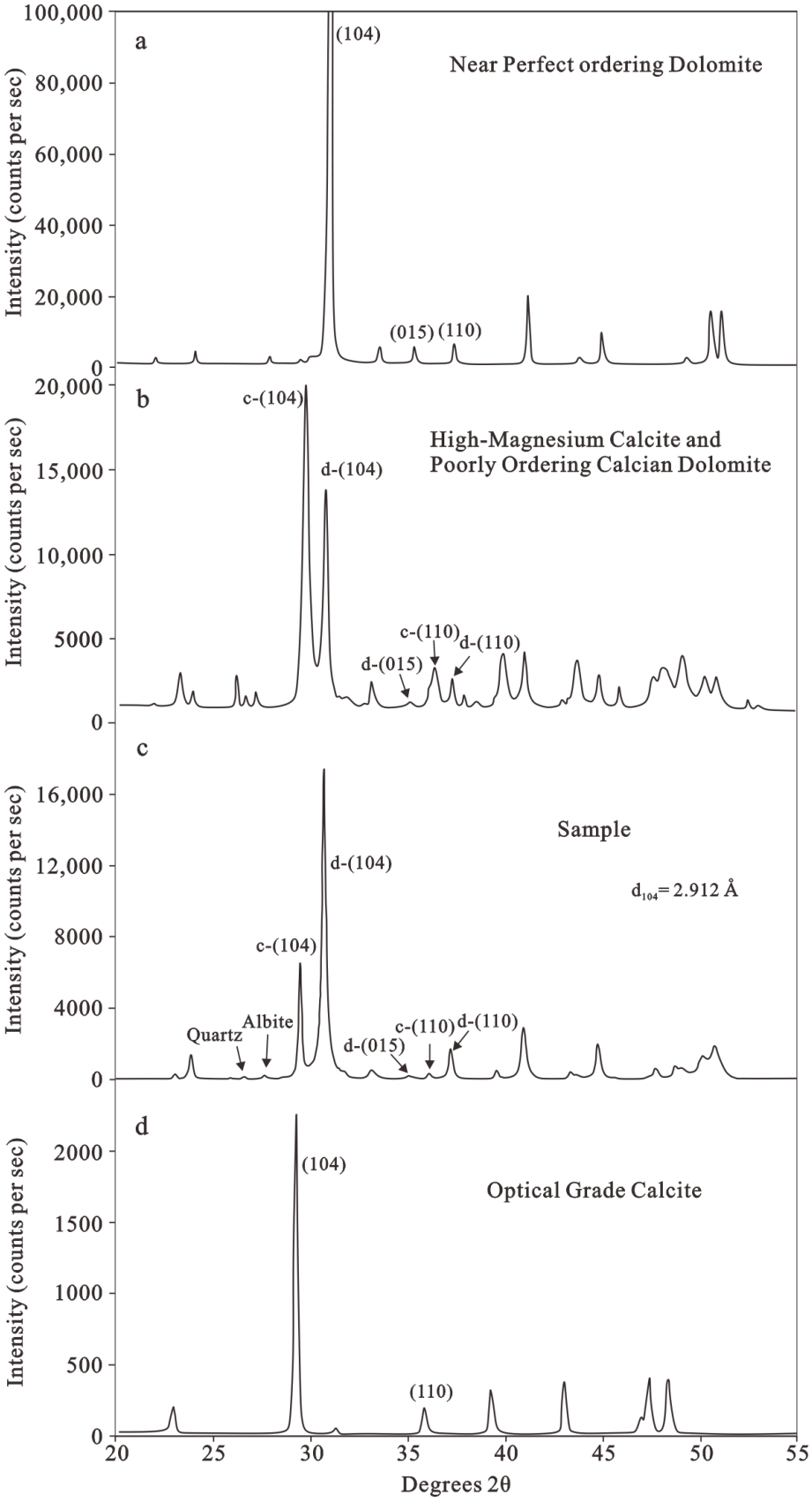

Figure 3. X-ray diffraction patterns of dolomite and calcite. Diffraction patterns of (**a**), (**b**) and (**d**) are from Gregg et al. [36]; (**c**) diffraction pattern of the sample Z1-15.

4.2. Characteristics of Ooids and Stable Isotopic Compositions

The sample consists of gray-white, well-sorted ooids (Figure 4a,b). The thin-section observation indicates that the sample is constituted of dolomitic ooids with calcite cement, and micritic ooids that are commonly dark and nearly opaque (Figure 4c,d). The calcite is red in the thin section, whereas the dolomitic ooids have no color (Figure 4d). All of the ooids display spherical or ovoid shapes (Figure 4c,d). The thin-section observation shows that the ooids have concentric or radial-concentric cortices (Figure 4c), whereas the dolomitic ooids display concentric cortices by observing the CL and ASB images (Figures 4e,f and 5a). The ooids mainly consist of micritic dolomite (Figures 5a,b and S2), whereas euhedral dolomite crystals develop on the surface of the ooids (Figure 5c,d). The minerals in the nucleus are mostly micritic dolomite with a minor clay mineral (kaolinite) and pyrite (Figures 5a,e,f and S2), and some are quartz or albite (Figures 5b and S2). The CL observation indicates that the calcite cement displays a light-orange luminescence and that the ooids show concentric dark and orange luminescence (Figure 4e,f). A total of 402 ooids were counted to identify grain sizes in the sample. The size of the ooids in the sample ranges from 144.7 μm to 1076 μm with a mean value of 431.3 μm, and with a majority of the ooids being a size from 244 μm to 544 μm (Figure 6a). The thickness of the cortices is from 41.4 μm to 312.7 μm with a mean value of 125 μm, and most have a thickness distributed from 71 μm to 161 μm (Figure 6b). The sample has a $\delta^{13}C_{VPDB}$ value of −0.7‰ and a $\delta^{18}O_{VPDB}$ value of −5.4‰.

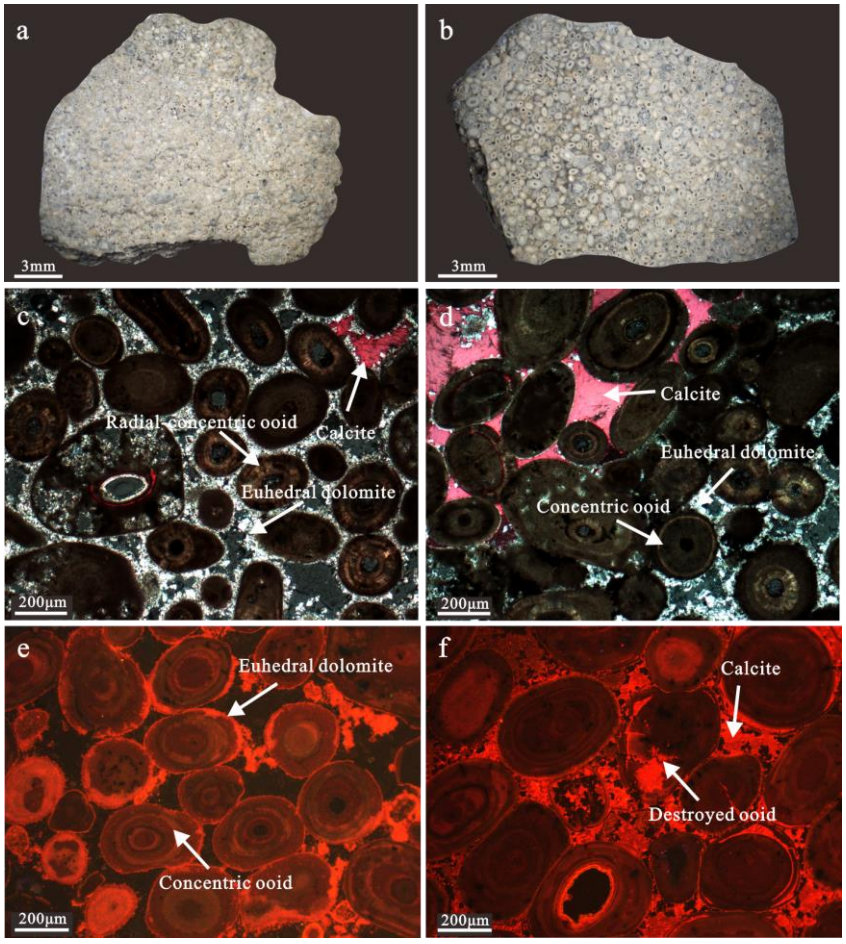

Figure 4. Hand sample Z1-15 and photomicrographs of the sample. (**a**) Photograph of the hand sample Z1-15, which consists of well sorted ooids; (**b**) stereoscopic photograph of the thin section of gray-white ooids; (**c**,**d**) cross-polarized-light images of the ooids show spherical or ovoid shapes ooids; (**e**,**f**) CL images reveal concentric dark and orange luminescence for ooids and light orange for calcite cement.

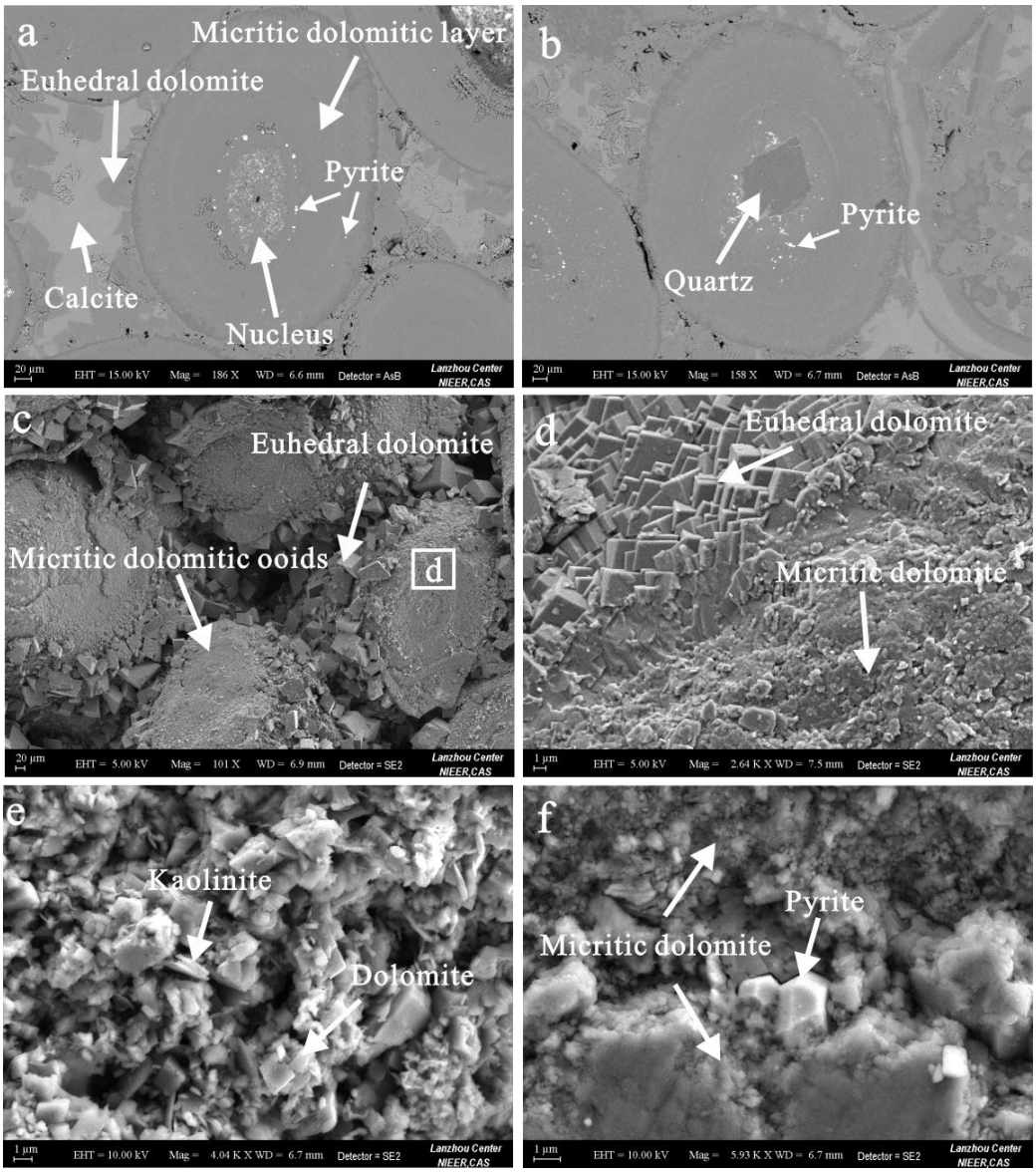

Figure 5. Scanning electron micrographs of the sample. (**a**,**b**) ASB images show concentric micritic dolomitic layer, micritic dolomitic and quartz nucleus, and pyrite in nucleus and cortices; (**c**) SE image shows that planar-e (euhedral) dolomite crystals were developed on the surface of ooids and in the pores; (**d**) SE image shows inner micritic dolomite with a plate pattern and outer euhedral dolomite crystal with a rhombic shape; (**e**) SE image shows minor kaolinite in the nucleus; (**f**) SE image shows that pyrites developed in the micritic dolomitic cortices.

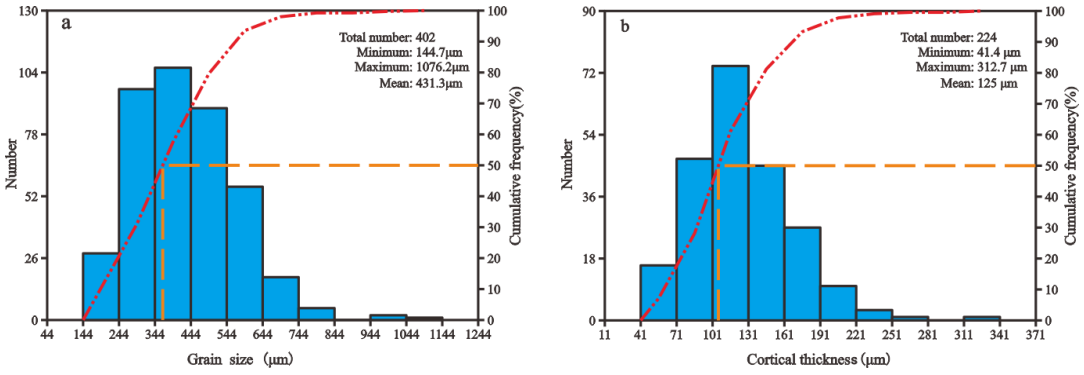

Figure 6. Distribution of ooid sizes and cortex thickness. (**a**) Distribution of ooid sizes; (**b**) distribution of cortex thickness.

5. Discussion

5.1. Primary Mineral of Ooids

The cortex layers of ooids from the modern marine environment are mostly composed of aragonite, and sometimes, they consist of high-Mg calcite in the marine hypersaline environment [37–39]. In contrast to marine ooids, the cortex layers of lacustrine ooids are generally aragonite [1]. As aragonite and high-magnesium calcite belong to the metastable mineral groups, they are almost completely transformed into low-magnesium calcite under the influence of diagenesis, therefor, ancient ooids are characterized by having calcite and low-magnesium calcite [1,17]. Dolomitic ooids are also found in ancient eras, such as the Neoproterozoic, the Paleoproterozoic, the Cambrian, etc [40–42]. Dolomitic ooids are most commonly formed via the replacement of aragonite or calcite, and retain some information about the original mineral characteristics and textures [17]. In the Qaidam Basin, the dolomitic ooids was found in the Pleistocene and shows the dolomite replacement of the aragonite, indicating that the primary minerals of the cortex layers of ooids are aragonite [24]. If the Ca-Mg carbonate is ordered, then it is dolomite; otherwise, it is not dolomite [43]. From the XRD patterns, it was identified that the Ca-Mg carbonate of this study was ordered, even though the ordering state of the dolomite is low. Our studied ooids consisted of nonplanar micritic dolomite and outward planar-e (euhedral) dolomite crystals (Figure 5c,d). The SEM images of the ooids do not show aragonite and its textures in the cortex layers of the ooids (Figure 5a,b). A few calcite found in the ooids' cortices occurred in some destroyed ooids, implying that the calcite was filled in during the later diagenesis, such as with the calcite cement in the sample, meaning that calcite is not the original mineral (Figure 4f). These features indicate that the primary minerals of the ooid cortices may be dolomite. The dolomite developed on the surface ooids and in the pores, presenting coarse euhedral crystals, which indicate that these dolomites were formed after the ooids were deposited.

Dolomite cannot be directly precipitated from modern seawater, and it is difficult synthesize in the laboratory under Earth surface conditions, which, due to hydration effects, hinder Mg^{2+} into the crystal lattice of the dolomite [44–46]. In contrast, recent studies show that dolomites can form at low temperatures through microbial-organic mediation with sulfide, silica, and clay minerals, which is supported by both laboratory experiments and field observations [47–55]. Sulfate-reducing bacteria play an important role in dolomite formation [47]. Sulfate reduction is an important redox process that assists in the conversion of SO_4^{2-} to HS^-. Dolomite occurs alongside the pyrite formed by sulfate-reducing bacteria in modern lakes [56,57]. The ASB images show the presence of micritic dolomite mixed with pyrites in the sample (Figure 5a,b). The elemental mapping of the ooids shows that nutritional elements such as P and Fe were detected, indicating that microbial remnants are present in the ooids (Figure 7). These findings indicate that the formation of dolomite is associated with sulfate-reducing bacteria. The CL properties of carbonate minerals reflect the spatial distribution of Fe and Mn ions [58]. In carbonate mineral, Mn^{2+} is the most important activator of CL, whereas Fe^{2+} is a quencher [59,60]. The CL images of the dolomitic ooids in the sample show a dark luminescence, which reflects more Fe^{2+} or low Mn^{2+} distributed in the ooids (Figure 4e,f). Combined with the Fe elemental mapping and the occurrence of the pyrite, more Fe^{2+} contents should lead to the ooids having a dark luminescence. This result also proves that micritic dolomite was formed through a reducing condition. Microbial sulfate reduction can produce dissolved sulfide in water, which enhances the Mg^{2+} incorporation into the calcitic structure and result in the precipitation of dolomite [51]. In addition, dissolved silica in water can also promote Mg^{2+} incorporation into the Ca-Mg carbonates, promoting dolomite nucleation and growth [55]. The elemental mapping of the ooids shows amounts of Si in the core (Figure 7). Thus, dissolved silica may be another important factor that enhances dolomite formation, with the exception of the microbial sulfate reduction. Dolomite formed at room temperature is often disordered dolomite or protodolomite [36,51,61]. When the sediments are buried, the

protodolomite is converted into ordered dolomite due to increasing temperature and pressure [36]. During an early burial, dolomite crystals formed on the surface ooids and in the pores (Figure 5d). With the dissolved silica and sulfide concentration drawn down in the pore water, the Mg^{2+} cannot enter into the calcitic structure, which leads to dolomite growth ceasing and calcitic cement occurring (Figure 5a).

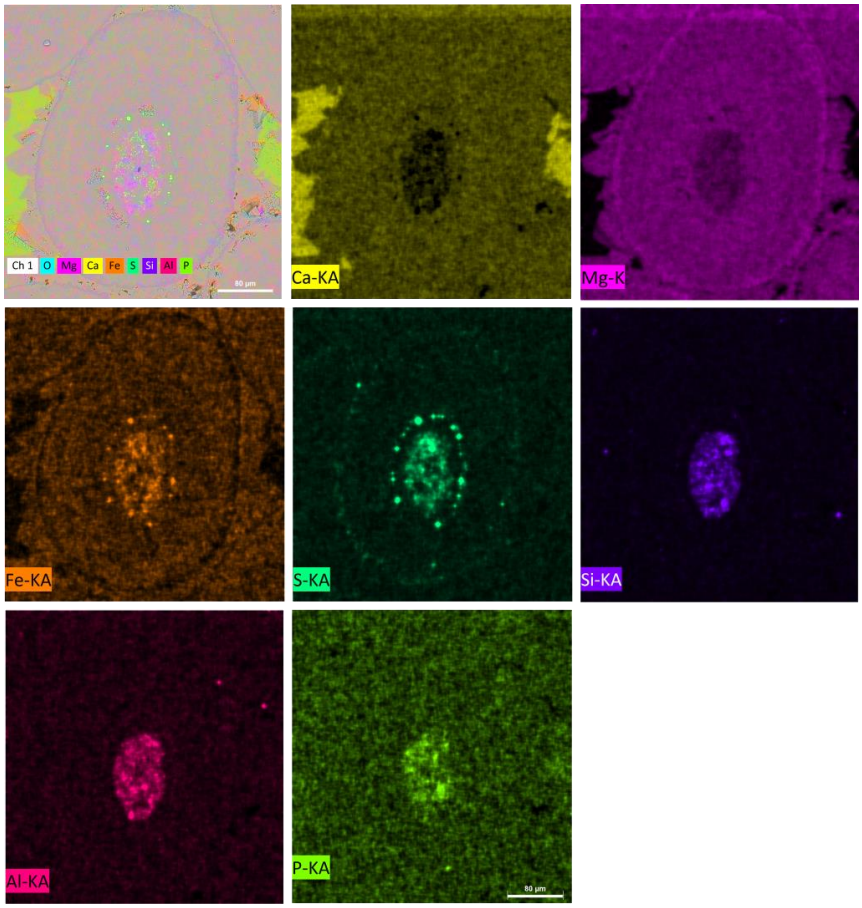

Figure 7. EDS elemental mapping of the ooids from Figure 5a.

5.2. Origin of Ooids

The mechanisms of ooid formation have been attributed to inorganic (physicochemical progress) or organic (biological progress) origins [1]. Based on the genesis of the dolomite above, it was found that dolomite is formed through microbial mediation. Therefore, the origin of ooids could be related to microorganisms. A biologically mediated process for ooid formation follows two processes: (1) a biologically induced mechanism (active mineralization) induces mineral precipitation though the microbial interaction with the environment; and (2) a biologically influenced mechanism (passive mineralization) provides mucilaginous material or extracellular polymeric substances (EPS) that act as a template for mineral precipitation [1]. SE images show that EPS was found in the cortex layers of ooids and nanodolomites mixed with EPS (Figure 8a). Through observations of the thin section milled by Ar ion, pyrites and EPS appear in the same area (Figure 8b). All together, these findings provide evidence that the formation of ooids is attributed to the biologically mediated mechanism. If the formation of ooids is entirely attributed to an organic process, they would grow in a quiet water environment with radial cortices [1]. Although some ooids present radial-concentric cortices, as seen in the thin section (Figure 4c), the dolomitic ooids display concentric cortices, as seen in the CL and ASB images (Figures 4e and 5a). Scanning electron microscopy analyses of ooid cortices reveal dolomite with plate morphologies, and nanograins along the edges of the plate (Figure 8c,d).

SE images of etched ooids show concentric laminations and nanograins aligned parallel to the laminae due to the nanocrystal dolomite aggregate running along lamellae directions (Figure 8e,f). These textural features indicate that the ooid cortices underwent textural changes. At the early stages of ooid accretion, the ooid cortices consisted of dolomitic nanograins with a random pattern (Figure 8g). The mutual impact of the ooids allows the nanograins to flatten and combine with each other to form plates that are oriented parallel to the laminae (Figure 8d,h). Therefore, ooid growth needs a strong hydrodynamic environment such as the surf zone, as this environment provides the force necessary for intergrain collision.

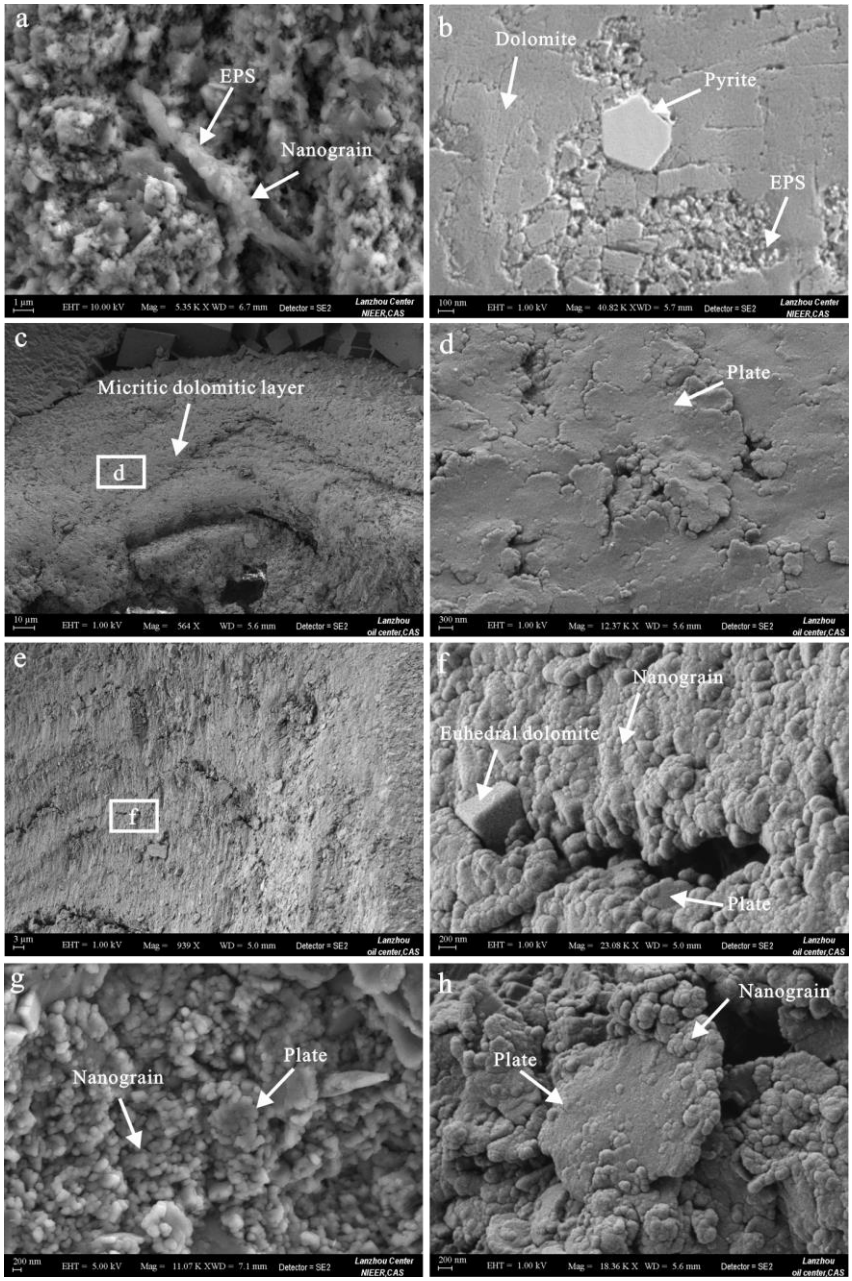

Figure 8. SE images of the ooids taken by scanning electron micrographs. (**a**) EPS occurs in the ooid cortices, where dolomite is within the EPS with a nanograin pattern; (**b**) all together, dolomite, EPS, and pyrite occur in the same area; (**c**) SEM image shows stacked dolomitic layers; (**d**) layer consists of dolomitic plates, which present deformation due to collision; (**e**) SEM image shows concentric laminations; (**f**) nanograins aligned parallel to the laminae, and the euhedral dolomite crystal was developed between layers; (**g**) dispersed nanograins and embryonic form of the plate; (**h**) dolomitic plate morphologies and nanograins along the edges of the plate.

The formation of ooids generally requires alternating agitated and resting stages [1,6]. These two stages often occur in the surf zone controlled by waves [1,6]. The textural characteristics of ooid cortices indicate that ooids are formed in a strong hydrodynamic environment, but microbial activity such as that of sulfate-reducing bacteria requires calm waters. Therefore, the surf zone of beaches with strong hydrodynamics does not meet the condition for ooid formation. Instead, the ooids could grow on the offshore lake floor away from the turbulent surf zones, where the sulfate-reducing bacteria and dissolved silica lead to nanograin mineral formation and the EPS matrix serves as the nucleation template for nanomineral precipitation. When the lake level draws down in the dry season, the ooids are transported from the calm microbially stabilized areas to surf zones, where the newly formed random nanograin minerals on the ooids are abraded to form flattened plates as a new polished layer. The sediment transport is repeated periodically until the ooids exceed a threshold size. This model of the ooid formation also occur in the marine environment and is named the "conveyor belt" model [11,62], which may be developed on windward beaches.

5.3. Implications for the Paleoenvironment

Although the lacustrine dolomites of the Quaternary age are found to span a wide range of geochemical and hydrological conditions, nearly all are from saline lakes [56]. The presence of dolomite ooids in this study suggests that the paleolake from the Pliocene may be a salt lake. However, the ooids formed in Pleistocene salt lakes in the Qaidam Basin consisted of aragonite and were cemented by halite and gypsum [24]. The occurrence of halite crystals, as the most common evaporative minerals, indicates that the Pleistocene lakes have a higher salinity than Pliocene lakes. Therefore, the shifting of ooid minerals from dolomite to aragonite may reflect the variation of the climate. The carbon and oxygen isotopic compositions of aragonitic ooids from the Pleistocene are similar to those of ooids from the Bahamas and New Zealand [63,64]. However, the carbon and oxygen isotopic compositions of our sample, which come from the boundary of the salt lake and belong to a brackish lake, are different from previously found compositions and present lower values (Figure 9). Variations of carbonate $\delta^{13}C$ and $\delta^{18}O$ are mainly attributed to the evaporation in the Qaidam Basin [25]. The evaporation of lake water was strengthened by climate drying, which results in the increase in the of $\delta^{13}C$ and $\delta^{18}O$ values of carbonates [65,66]. Differences in the mineral composition and isotopic composition indicate that the Pliocene lakes have a lower salinity and are more humid than Pleistocene lakes. Fang and Xu [67] also indicated that the oscillatory appearance in the types of sedimentary carbonate can be used to interpret paleoenvironmental changes. Differences in the silicate weathering can lead to variation in the input of silica into the lake [68]. Strong silicate weathering produces more silica in the lake and enhances the dolomite precipitation; conversely, weak silica weathering precipitates calcite or aragonite [68]. Therefore, the change from dolomite ooids in the Pliocene to aragonite ooids in the Pleistocene might also be due to dissolved silica concentration changes in the lake.

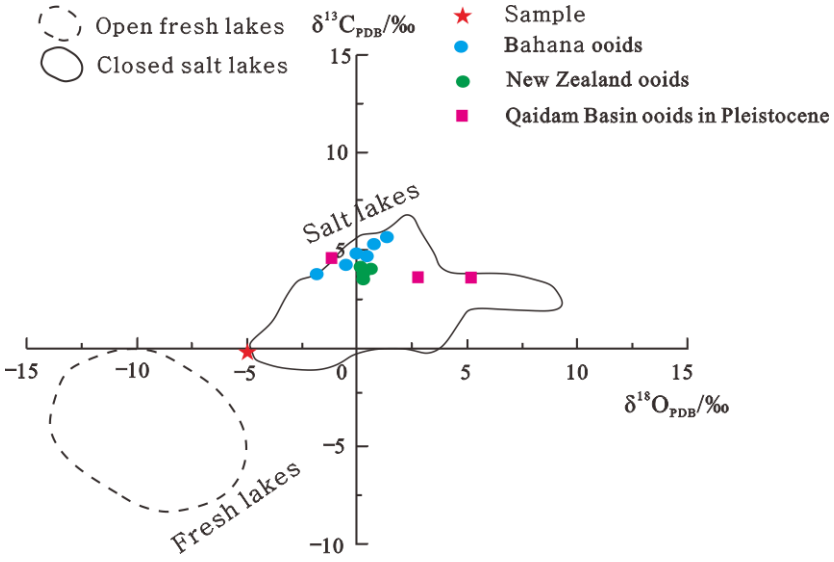

Figure 9. Scatter plot of carbon versus oxygen isotopic compositions of ooids (modified from Sun et al. [24]). Carbon and oxygen isotopic data of the Bahamas ooids, the New Zealand ooids and the Pleistocene ooids in the Qaidam Basin are from Rankey et al. [64], Duguid et al. [63] and Sun et al. [24], respectively.

Climate change and tectonic activity in the Qaidam Basin can control the oscillations of authigenic minerals, such as various evaporite and clay minerals [20]. During the Pliocene–Quaternary, two intense main uplifts in the Qaidam Basin occurred at 5.3–4.5 Ma and ~3.6 Ma [19,69,70]. At 5.3 Ma, the climate is already dry, but the aridification is not serious [21]. The appearance of *Pediastrum* in the Yahu Anticline, which occurs frequently in freshwater environments, indicates relatively wet conditions during this period [21]. Heermance et al. [30] indicated that the lake in the central Qaidam Basin is a freshwater lake at 4.2 Ma. Thus, the lake water gradually changes from fresh water to brackish water during the Pliocene. It is consistent with the lake water conditions indicated by the carbon and oxygen isotopes of ooids in this study. During this period, the Qaidam Basin experienced a relatively high temperature [20], which enhanced the silicate weathering and provided more dissolved silica to be inputted into the lake [68]. When the water reached the chemical conditions that can precipitate dolomite, the dolomite ooids were formed due to the participation of sulfate-reducing bacteria and dissolved silica. A drought event occurred at 3.6 Ma owing to both global cooling and the Tibetan Plateau uplift [19,20], which caused a long-term stepwise drying of the Qaidam Basin after the late Pliocene [21]. A widespread distribution of evaporative minerals such as calcite, aragonite, and gypsum occurred during this period reflecting an abrupt change in the paleolacustrine chemistry [20]. Notably, during the Mid-Pleistocene Climate Transition event, global cooling led to the global ice volume increasing by ~15% [71], which resulted in decreasing strength of silicate weathering and, ultimately, less dissolved silica [68]. Reduced silica input into the lake resulted in aragonite precipitation in the lake water and the formation of aragonite ooids. The change in the climate led to the variation in the microbial activity and dissolved silica concentrations in the water, which could catalyze dolomite growth [55,67]. The variations in the mineral compositions and isotopes of ooids in the Pliocene and Pleistocene correspond to the different uplift stages of the Qaidam Basin. Therefore, ooids can be used as an indicator of climatic change and uplift history for the Tibet Plateau.

6. Conclusions

1) The ooids formed in the Pliocene Shizigou Formation in the Qaidam Basin mainly consist of micritic dolomite that is poorly ordered. The nuclear minerals are mostly micritic dolomite with a minor clay mineral and pyrite. The thin-section and SEM observations combined with CL indicate that the primary mineral of the ooid cortices

is dolomite. The micritic dolomite was formed through a reducing condition, and its formation was related to the presence of sulfate-reducing bacteria and dissolved silica. The euhedral dolomite crystals were formed in the pore water after the ooids were deposited.

2) The formation of the dolomitic ooids in the Shizigou Formation occurred according to the "conveyor belt" model. The ooids grew on the offshore lake floor, where nanominerals were precipitated on the EPS due to the involvement of sulfate-reducing bacteria and other microbes. Then, the ooids were reformed under strong hydrodynamic surf zones, where the random nanograin minerals were abraded to form flattened plates as a new polished layer. The sediment transport was repeated periodically until the ooids exceeded a threshold size.
3) Ooids from the different uplift stages of the Qaidam Basin (in the Pliocene and Pleistocene) have variations in mineral compositions and the carbon and oxygen isotopes. The minerals of the ooid cortices changed from Pliocene dolomite to Pleistocene aragonite. The $\delta^{13}C$ and $\delta^{18}O$ values of the Pleistocene carbonates are higher than those of the Pliocene. These differences indicate that the Pliocene lakes had a lower salinity and were more humid than Pleistocene lakes. Ooids may be an effective proxy for reflecting the climatic change and uplift history of the Tibet Plateau.

Supplementary Materials: The following supporting information can be downloaded at: https://www.mdpi.com/article/10.3390/min12121586/s1, Figure S1: X-ray diffraction patterns of the sample; Figure S2: EDS spectra for minerals corresponding to those of Figure 5.

Author Contributions: Conceptualization, L.H. and J.J.; methodology, L.H. and H.T.; software, X.M. and J.C.; validation, L.H. and J.J.; formal analysis, L.H., J.J., and J.Q.; investigation, L.H., J.J., and J.Q.; data curation, J.C. and X.M.; writing—original draft preparation, L.H. and H.T.; writing—review and editing, L.H., J.J., and H.T.; supervision, S.L.; funding acquisition, L.H., J.J., and J.C. All authors have read and agreed to the published version of the manuscript.

Funding: This research was funded by the Second Tibetan Plateau Scientific Expedition and Research Program (STEP), grant number 2019QZKK0704, and the Effective Reservoirs of Deep Brine in Tertiary Anticline Structural Area in Qaidam Basin.

Data Availability Statement: Not applicable.

Conflicts of Interest: The authors declare no conflicts of interest.

References

1. Diaz, M.R.; Eberli, G.P. Decoding the mechanism of formation in marine ooids: A review. *Earth-Sci. Rev.* **2019**, *190*, 536–556.
2. Ball, M.M. Carbonate sand bodies of florida and the bahamas. *J. Sediment. Petrol.* **1967**, *37*, 556–591.
3. Harris, P.M.; Halley, R.B.; Lukas, K.J. Endolith microborings and their preservation in Holocene-Pleistocene (Bahamas-Florida) ooids. *Geology* **1979**, *7*, 216–220.
4. Li, F.; Yan, J.X.; Algeo, T.; Wu, X. Paleoceanographic conditions following the end Permian mass extinction recorded by giant ooids (Moyang, South China). *Glob. Planet. Chang.* **2013**, *105*, 102–120.
5. Liu, X.; Chen, X.; Tostevin, R.; Yao, H.; Han, K.; Guo, H.; Jafarian. A. Post-depositional modification of carbonate ooids by sulfate-reducing bacteria: Evidence from the Lower–Middle Jurassic, Tethyan Himalayas of southern Tibet. *Sed. Geol.* **2021**, *426*, 106027.
6. Davies, P.J.; Bubela, B.; Ferguson, J. The formation of ooids. *Sedimentology* **1978**, *25*, 703–730.
7. Rankey, E.C.; Reeder, SL. Holocene ooids of Aitutaki Atoll, Cook Islands, South Pacific. *Geology* **2009**, *37*, 971–974.
8. Diaz, M.R.; Swart, P.K.; Eberli, G.P.; Oehlert, A.M.; Devlin, Q.; Saeid, A.; Altabet, M.A. Geochemical evidence of microbial activity within ooids. *Sedimentology* **2015**, *62*, 2090–2112.
9. Diaz, M.R.; Eberli, G.P.; Blackwelder, P.; Phillips, B.; Swart, P.K. Microbially mediated organomineralization in the formation of ooids. *Geology* **2017**, *45*, 771–774.
10. Li, F.; Yan, J.; Burne, R.V.; Chen, Z.Q.; Algeo, T.J.; Zhang, W.; Tian, L.; Gan, Y.; Liu, K.; Xie, S. Paleo-seawater REE compositions and microbial signatures preserved in laminae of lower Triassic ooids. *Palaeogeogr. Palaeoclimatol. Palaeoecol.* **2017**, *486*, 96–107.
11. O'Reilly, S.S.; Mariotti, G.; Winter, A.R.; Newman, S.A.; Matys, E.D.; McDermott, F.; Pruss, S.B.; Bosak, T.; Summons, R.E.; Klepac-Ceraj, V. Molecular biosignatures reveal common benthic microbial sources of organic matter in ooids and grapestones from Pigeon Cay, the Bahamas. *Geobiology* **2017**, *15*, 112–130.

12. Batchelor, M.T.; Burne, R.V.; Henry, B.I.; Li, F.; Paul, J. A biofilm and organomineralisation model for the growth and limiting size of ooids. *Sci. Rep.* **2018**, *8*, 559.
13. Opdyke, B.N.; Wilkinson, B.H. Paleolatitude distribution of Phanerozoic marine ooids and cements. *Palaeogeogr. Palaeoclimatol. Palaeoecol.* **1990**, *78*, 135–148.
14. Sumner, D.Y.; Grotzinger, J.P. Numerical modeling of ooid size and the problem of Neoproterozoic giant ooids. *J. Sediment. Res.* **1993**, *63*, 974–982.
15. Thorie, A.; Mukhopadhyay, A.; Banerjee, T.; Mazumdar, P. Giant ooids in a Neoproterozoic carbonate shelf, Simla Group, Lesser Himalaya, India: An analogue related to Neoproterozoic glacial deposits. *Mar. Pet. Geol.* **2018**, *98*, 582–606.
16. Lu, C.; Li, F.; Oehlert, A.M.; Li, J.; Zou, H. Reconstructing paleoceanographic conditions during the middle Ediacaran: Evidence from giant ooids in South China. *Precambrian Res.* **2020**, *351*, 105945.
17. Li, F.; Wu, S.; Liu, K. Identification of Ooid Primary Mineralogy: A clue for understanding the variation in paleo-oceanic chemistry. *Acta Sedimentol. Sin.* **2015**, *33*, 500–511.
18. Land, L.S.; Behrens, E.W.; Frishman, S.A. The ooids of Baffin Bay, Texas. *J. Sediment. Petrol.* **1979**, *49*, 1269–1278.
19. Fang, X.M.; Zhang, W.L.; Meng, Q.Q.; Gao, J.P.; Wang, X.M.; King, J.; Song, C.H.; Dai, S.; Miao, Y.F. High-resolution magneto stratigraphy of the Neogene Huaitoutala section in the eastern Qaidam Basin on the NE Tibetan Plateau, Qinghai Province, China and its implication on tectonic uplift of the NE Tibetan Plateau. *Earth Planet. Sci. Lett.* **2007**, *258*, 293–306.
20. Fang, X.; Li, M.; Wang, Z.; Wang, J.; Li, J.; Liu, X. Oscillation of mineral compositions in Core SG-1b, western Qaidam Basin, NE Tibetan Plateau. *Sci. Rep.* **2016**, *6*, 32848.
21. Wu, F.L.; Fang, X.M.; Herrmann, M.; Mosbrugger, V.; Miao, Y.F. Extended drought in the interior of Central Asia since the Pliocene reconstructed fromsporopollen records. *Glob. Planet. Chang.* **2011**, *76*, 16–21.
22. Zhang, W.; Appel, E.; Fang, X.; Yan, M.; Song, C.; Cao, L. Paleoclimatic implications of magnetic susceptibility in late Pliocene–Quaternary sediments from deep drilling core SG-1 in the western Qaidam Basin (NE Tibetan Plateau). *J. Geophys. Res.* **2012**, *117*, B06101.
23. Lu, Y.; Fang, X.; Appel, E.; Wang, J.; Herb, C.; Han, W.; Wu, F.; Song, C. A 7.3–1.6 Ma grain size record of interaction between anticline uplift and climate change in the western Qaidam Basin, NE Tibetan Plateau. *Sed. Geol.* **2015**, *319*, 40–51.
24. Sun, Y.; Li, Y.; Li, L.; He, H. Preservation of cyanobacterial UVR-shielding pigment scytonemin in carbonate ooids formed in Pleistocene salt lakes in the Qaidam Basin, Tibetan Plateau. *Geophys. Res. Lett.* **2019**, *46*, 10375–10383.
25. Han, W.; Fang, X.; Ye, C.; Teng, X.; Zhang, T. Tibet forcing Quaternary stepwise enhancement of westerly jet and central Asian aridification: Carbonate isotope recordsfrom deep drilling inthe Qaidam salt playa, NETibet. *Glob. Planet. Chang.* **2014**, *116*, 68–75.
26. Cheng, Feng.; Jolivet, M.; Guo, Z.; Wang, L.; Zhang, C.; Li, X. Cenozoic evolution of the Qaidam basin and implications for the growth of the northern Tibetan plateau: A review. *Earth-Sci. Rev.* **2021**, *220*, 103730.
27. Zhu, L.; Wang, C.; Zheng, H.; Xiang, F.; Yi, H.; Liu, D. Tectonic and sedimentary evolution of basins in the northeast of Qinghai-Tibet Plateau and their implication for the northward growth of the Plateau. *Palaeogeogr. Palaeoclimatol. Palaeoecol.* **2006**, *241*, 49–60.
28. Jian, X.; Guan, P.; Zhang, D.W.; Zhang, W.; Feng, F.; Liu, R.J.; Lin, S.D. Provenance of Tertiary sandstone in the northern Qaidam basin, northeastern Tibetan Plateau: Integration of framework petrography, heavy mineral analysis and mineral chemistry. *Sed. Geol.* **2013**, *290*, 109–125.
29. Sun, G.; Wang, M.; Guo, J.; Wang, Y.; Yang, Y. Geochemical Significance of Clay Minerals and Elements in Paleogene Sandstones in the Center of the Northern Margin of the Qaidam Basin, China. *Minerals* **2020**, *10*, 505.
30. Heermance, R.V.; Pullen, A.; Kapp, P.; Garzione, C.N.; Bogue, S.; Ding, L.; Song, P. Climatic and tectonic controls on sedimentation and erosion during the Pliocene–Quaternary in the Qaidam Basin (China). Geol. *Soc. Am. Bull.* **2013**, *125*, 833–856.
31. Goldsmith, J.R.; Graf, D.L. Structural and compositional variations in some natural dolomites. *J. Geol.* **1958**, *66*, 678–693.
32. Fang, Y.; Xu, H. A New Approach to Quantify the Ordering State of Protodolomite Using XRD, TEM, and Z-Contrast Imaging. *J. Sediment. Res.* **2019**, *89*, 537–551.
33. Graf, D.L.; Goldsmith, J.R. Some hydrothermal syntheses of dolomite and protodolomite. *J. Geol.* **1956**, *64*, 173–186.
34. Chave, K.E. Factors influencing the mineralogy of carbonate sediments. *Limnol. Oceanogr.* **1962**, *7*, 218–223.
35. Chave, K.E. A solid solution between calcite and dolomite. *J. Geol.* **1952**, *60*, 190–192.
36. Gregg, J.M.; Bish, D.L.; Kaczmarek, S.E.; Machel, H.G. Mineralogy, nucleation and growth of dolomite in the laboratory and sedimentary environment: A review. *Sedimentology* **2015**, *62*, 1749–1769.
37. Marshall, J.F.; Davies, P.J. High-magnesium calcite ooids from the Great Barrier Reef. *J. Sediment. Res.* **1975**, *45*, 285–291.
38. Milliman, J.D.; Barreto, H.T. Relict magnesian calcite oolite and subsidence of the Amazon shelf. *Sedimentology* **1975**, *22*, 137–145.
39. Flügel, E. *Microfacies of Carbonate Rock: Analysis, Interpretation and Application*, 2rd ed.; Springer: Berlin, German, 2010; p. 984.
40. Trower, E.J.; Grotzinger, J.P. Sedimentology, diagenesis, and stratigraphic occurrence of giant ooids in the Ediacaran Rainstorm Member, Johnnie Formation, Death Valley region, California. *Precambrian Res.* **2010**, *80*, 113–124.

41. Banerjee, A.; Słowakiewicz, M.; Majumder, T.; Khan, S.; Patranabis-Deb, S.; Tucker, M.E.; Saha, D. A Palaeoproterozoic dolomite (Vempalle Formation, Cuddapah Basin, India) showing Phanerozoic-type dolomitisation, *Precambrian Res.* **2019**,*328*, 9–26.
42. Guo, Q.; Jin, Z.; Zhu, X.; Shi, S.;·Wang, J.;·Wang, J.; Li, Y.; Li, S. Characteristics and mechanism of dolomitization in the ooids of the Cambrian Zhangxia Formation, Xiaweidian, China. *Carbonates Evaporites* **2020**, *35*, 7.
43. Land, L.S. The isotopic and trace element geochemistry of dolomite: The state of the art. *SEPM Spec. Publ.* **1980**, *28*, 87–110.
44. Lippmann, F. Sedimentary Carbonate Minerals, Rocks and Inorganic Materials. In *Monograph Series of Theoretical and Experimental Studies 4*; Springer: Berlin, German, 1973; p. 228.
45. Warren, J. Dolomite: Occurrence evolution and economically important associations. *Earth Sci. Rev.* **2000**, *52*, 1–81.
46. Rodriguez-Blanco, J.D.; Shaw, S.; Benning, L.G. A route for the direct crystallization of dolomite. *Am. Mineral.* **2015**, *100*, 1172–1181.
47. Vasconcelos, C.; McKenzie, J.A.; Warthmann, R.; Bernasconi, S.M. Microbial mediation as a possible mechanism for natural dolomite formation at low temperatures. *Nature* **1995**, *377*, 220–222.
48. Wright, D.T.; Oren, A. Nonphotosynthetic bacteria and the formation of carbonates and evaporites through time. *Geomicrobiol. J.* **2005**, *22*, 27–53.
49. Qiu, X.; Wang, H.; Yao, Y.; Duan, Y. High salinity facilitates dolomite precipitation mediated by Haloferax volcanii DS52. *Earth Planet. Sci. Lett.* **2017**, *472*, 197–205.
50. Zhang, F.; Xu, H.; Konishi, H.; Shelobolina, E.S.; Roden, E.E. Polysaccharide-catalyzed nucleation and growth of disordered dolomite: A potential precursor of sedimentary dolomite. A*m. Miner.* **2012**, *97*, 556–567.
51. Zhang, F.; Xu, H.; Konishi, H.; Kemp, J.M.; Roden, E.E.; Shen, Z. Dissolved sulfide-catalyzed precipitation of disordered dolomite: Implications for the formation mechanism of sedimentary dolomite. *Geochim. Cosmochim. Acta* **2012**, *97*, 148–165.
52. Zhang, F.; Xu, H.; Shelobolina, E.S.; Konishi, H.; Converse, B.; Shen, Z.; Roden, E.E. The catalytic effect of bound extracellular polymeric substances excreted by anaerobic microorganisms on Ca-Mg carbonate precipitation: Implications for the "dolomite problem." *Am. Miner.* **2015**, *100*, 483–494.
53. Xu, H.; Zhou, M.; Fang, Y.; Teng, H.H. Effect of Mica and Hematite (001) Surfaces on the Precipitation of Calcite. *Minerals* **2018**, *8*, 17.
54. Liu, D.; Xu, Y.; Papineau, D.; Yu, N.; Fan, Q.; Qiu, X.; Wang, H. Experimental evidence for abiotic formation of low-temperature proto-dolomite facilitated by clay minerals. *Geochim. Cosmochim. Acta* **2019**, *247*, 83–95.
55. Fang, Y.; Xu, H. Dissolved silica-catalyzed disordered dolomite precipitation. *Am. Miner.* **2022**, *107*, 443–452.
56. Last, W.M. Lacustrine dolomite-an overview of modern, Holocene, and Pleistocene occurrences. *Earth-Science Rev.* **1990**, *27*, 221–263.
57. Yu, B.; Dong, H.; Jiang, H.; Li, S.; Liu, Y. Discovery of Spheric Dolomite Aggregations in Sediments from the Bottom of Qinghai Lake and Its Significance for Dolomite Problem. *Geoscience* **2007**, *21*, 66–70.
58. Bruhn, F.; Bruckschen, P.; Richter, DK.; Meijer, J.; Stephan, A.; Veizer, J. Diagenetic history of sedimentary carbonates: Constraints from combined cathodoluminescence and trace element analyses by micro-PIXE. *Nucl Instr Meth Phys Res* **1995**, *B104*, 409–414.
59. Mariano, A.N. Some further geological applications of cathodoluminescence. In *Cathodoluminescence of geological materials*, Marshall, J.D., Ed.; Unwin Hyman: Boston, MA, USA, 1988; pp. 94–123.
60. Pagel, M.; Barbin, V.; Blanc, P.; Ohnenstetter, D. *Cathodoluminescence in Geosciences*; Springer: Berlin, German, 2000; p. 514.
61. Kaczmarek, S.E.; Thornton, B.P. The effect of temperature on stoichiometry, cation ordering, and reaction rate in high-temperature dolomitization experiments. *Chem. Geol.* **2017**, *468*, 32–41.
62. Mariotti, G.; Pruss, S.B.; Klepac-Ceraj, V.; Summons, R.E.; Newman, S.A.; Bosak, T. Where Is the Ooid Factory? In Proceedings of theAmerican Geophysical Union Fall Meeting, San Francisco, CA, USA, 15–19 December 2014.
63. Duguid, S.M.A.; Kyser, T.K. James, N.P.; Rankey, E.C. Microbes and ooids. *J. Sediment. Res.* **2010**, *80*, 236–251.
64. Rankey, E.C.; Reeder, S.L. Holocene oolitic marine sand complexes of the Bahamas. *J. Sediment. Res.* **2011**, *81*, 97–117.
65. Talbot, M.R. A review of the palaeohydrological interpretation of carbon and oxygen isotopic ratios in primary lacustrine carbonates. *Chem. Geol. Isot. Geosci. Sect.* **1990**, *80*, 261–279.
66. Leng, M.J.; Marshall, J.D. Palaeoclimate interpretation of stable isotope data from lake sediment archives. *Quat. Sci. Rev.* **2004**, *23*, 811–831.
67. Fang,Y.; Xu, H. Study of an Ordovician Carbonate with alternating dolomite–calcite laminations and its implication for catalytic effects of microbes on the formation of Sedimentary dolomite. *J. Sediment. Res.* **2018**, *88*, 679–695.
68. Fang,Y.; Xu, H. Coupled dolomite and silica precipitation from continental weathering during deglaciation of the Marinoan Snowball Earth. *Precambrian Res.* **2022**, *380*, 106824.
69. Li, J.J.; Fang, X.M. Uplift of Tibetan Plateau and environmental changes. *Chinese Sci. Bull.* **1999**, *44*, 2117–2124.
70. Sun, J.M.; Zhu, R.X.; Bowler, J. Timing of the Tianshan Mountains uplift constrained by magnetostratigraphic analysis of molasses deposits. Earth Planet. *Sci. Lett.* **2004**, *219*, 239–253.
71. Li, J.; Li, M.; Fang, X.; Zhang, G.; Zhang, W.; Liu, X. Isotopic composition of gypsum hydration water in deep Core SG-1, western Qaidam basin (NE Tibetan Plateau), implications for paleoclimatic evolution. *Glob. Planet. Chang.* **2017**, *155*, 70–77.